Lasers in Manufacturing Conference 2025

Depth measurement performance of OCT during laser welding with single-mode core and ring beam configurations

Serge André Dib[a*], Tianqiu Xu[a], Daniele Colombo[b], Ali Gökhan Demir[a]

[a]*Department of Mechanical Engineering, Politecnico di Milano, Via La Masa 1, 20158 Milan, Italy*
[b]*BLM Group Adige Spa, Via Per Barco 11, 38056 Levico Terme, Italy*

Abstract

The demand for precise measurements of high-speed laser welding depth is increasing due to growing e-mobility applications. Optical coherence tomography (OCT) can measure keyhole depth in real time. Newer fiber laser generations, ideal for such applications, allow single-mode core/ring configurations. However, OCT's usability with small keyhole apertures may cause measurement inconsistencies. This work proposes a systematic analysis of signal behaviour using a contemporary fiber laser with a single-mode core and a ring with separate power control, producing focal core and ring sizes of 40 µm and 285 µm, respectively. Bead-on-plate experiments were conducted on 5 mm thick EN AW-1050 Al-alloy. Core and ring power levels were systematically analysed along with scan speeds. The OCT focal beam of 35 µm was aligned with the laser beam for different process parameters. Keyhole depth was compared to molten seam depth from metallographic cross-sections. Alignment protocols were showcased to highlight the sensitivity of OCT measurements.

Keywords: Optical coherence tomography; electric mobility; online monitoring; beam shaping

1. Introduction

Driven by the accelerated electrification of automobiles, reliable joining technologies have become more important (Demir et al., 2023). Laser beam welding (LBW) emerges as a key technology, therefore. Compared to conventional joining technologies, i.e. resistance spot welding, arc welding, and ultrasonic welding, LBW holds several advantages. It allows smaller processing zones generating reduced heat-affected zones. LBW has also been a key technology in electric mobility applications due to its adaptability to different weld joints, thicknesses, and material combinations. Battery systems, electric drives, and high-power electronics require permanent connections produced by rapid welding operations with scan speeds in the order of a few hundreds of mm/s, where often single-mode laser beams at several kilowatts of power are used. An important factor in weld quality is the weld depth and its constancy. Another important factor regards the generation of spatter, which may result in porosity and undercuts in the weld seam as well as contaminating the welded product. Contemporary industrial laser solutions provide core/ring beam combinations and inline depth measurement devices that can be adapted to electric mobility applications.

Several methods have been proposed to monitor the weld depth, based mainly on visual imaging, acoustic signals and indirect observation of optical radiation (Xie et al., 2023). Optical coherence tomography (OCT) has become a robust choice in recent years as it can measure the weld depth in real-time. For deep penetration welding, the beam of OCT is deployed co-axially with the laser beam (Webster et al., 2010). When the OCT beam is aligned properly towards the keyhole's bottom, the technology provides fast and direct measurement of the keyhole depth. The challenge in the application is in the precise alignment of the OCT beam within the capillary opening for a reliable and appropriate optical path length and data acquisition to measure the weld depth (Mittelstädt et al., 2019). As a matter of fact, the keyhole depth is usually insignificantly lower than the weld depth (Blug et al., 2011). Some studies indicate a negligible molten film at the bottom of the keyhole (Miyagi et al., 2017). In consequence, OCT monitoring of the keyhole depth can be considered as a direct indicator of the weld depth.

The quality of the OCT keyhole depth measurement depends intrinsically on the welding conditions and, hence, the process parameters used and the spatial offset with respect to the laser beam applied. Keyhole fluctuations and instabilities can potentially affect the OCT measurements (Boley et al.,2013). In general, the keyhole shape, tilt, and volume are influenced by the choice of laser process parameters and materials. Process disturbances might render the OCT sensor data unreliable due to the generated unstable capillary, on the one hand, causing signal fluctuations and measurement errors (Dorsch et al., 2016). On the other hand, a proper alignment of the OCT beam within the keyhole bottom is required. The applicability of OCT measurements in laser welding often calls for wide keyhole openings allowing the OCT beam to reach the keyhole bottom without obstacles in the optical path. Moreover, relatively low weld speeds (<100 mm/s) are employed allowing a reasonable reconstruction of the weld depth with the temporal sampling frequency of the device in the range of 100 kHz. For high-speed welding conditions used in electric mobility applications, the added ring to the core beam can allow for a wider opening of the keyhole. Accordingly, accurate calibration procedures are required to exploit the measurement system correctly with the available sampling frequencies.

In literature, most of the works concentrate on high power levels from 2 to 6 kW combined with low welding speeds from 10 to 200 mm/s, eventually generating a keyhole shape that renders the OCT beam alignment relatively simpler. The use of OCT during the welding using a single-mode beam has been studied sparingly due to difficulty of aligning the beam spatially and temporally in a small capillary aperture (Schmoeller et al., 2019 and He et al., 2024). For most of the works, the process parameters were selected to render the OCT beam alignment easier by enlarging the keyhole.

OCT weld depth monitoring for remote laser welding of battery tab connectors implementing a core beam complemented with a ring beam has been investigated by Sokolov et al., 2020. Thin foil stacks of Al-Cu, with thicknesses of 450 µm and 300 µm respectively, were welded using an adjustable ring-mode laser. The study investigated the variation effects of the core and ring powers—using core power levels between 650 and 800 W and ring power levels between 50 and 1500 W at a weld speed of 175 mm/s. The ring profile helped in controlling the temperature distribution, rendering the keyhole both more stable and larger. The OCT measurement error of the weld penetration depth was reduced significantly compared to the same measurements for which only the core beam was adopted. Furthermore, in-situ keyhole monitoring using a highly brilliant single-mode beam with a spot diameter of 55 µm, has been reported in the literature (Schmoeller et al., 2019) using power levels between 1.5 and 2.7 kW and a weld speed of 165 mm/s. The results showed a high dependency of the OCT signal quality on the different process parameters. Notable differences between the real weld depth and the measured weld depth were observed when aiming for deeper welds with the single-mode core beam. In general, a small laser beam diameter and a low penetration depth complicate a steady and precise measurement of the keyhole (Hollatz et al., 2020). The importance of the calibration of the OCT beam position is apparent for industrial applications as well as a greater understanding of the process dynamics. Moreover, for measuring the keyhole depth through small keyhole apertures at high scan speeds, such procedures are crucial for reliable and meaningful measurements. As a matter of fact, correct beam alignment procedures are crucially important to fully exploiting the potential of this technology when adopted in electric mobility applications. To the authors' knowledge, OCT keyhole depth measurement with single-mode fiber lasers at scan speeds of several hundreds of mm/s has not been previously reported in literature.

In this work, the influencing factors on OCT measurement signals were investigated for a robust and reliable process monitoring in remote LBW. Bead-on-track experiments were conducted using a fiber laser with single-mode core and ring configuration on Al-alloy samples. The feasibility of using OCT to measure small capillary depths at relatively high scan speeds was assessed. OCT beam alignment procedures were presented to show the sensibility of the process during welding with speeds of up to 800 mm/s without and with added ring power that is often used as aid to enhance measurement capability. The measurements were compared to melt track depths made on metallurgical cross-sections to assess the influence of the alignment procedure.

2. Experimental setup

2.1. Laser source and OCT system

A schematic of the experimental setup is shown in Figure 1. A fiber laser with a core/ring configuration emitting at a wavelength of 1070 nm was used (YLS-2000/4000-SM-AMB, IPG Photonics, Cambridge, CA, USA). The delivery fiber was characterized with a single-mode core beam with a fiber core diameter of 14 µm complemented with a ring beam with an inner diameter of 40 µm and an outer diameter of 100 µm. The power content within the single-mode core and the ring portions could be addressed separately up to 2 kW and 4 kW, respectively. The resulting focal diameters were measured at 40 µm for the core beam, and 115 µm and 285 µm for the inner and outer ring beams, with a beam profiler (SP90609 BeamPeek, Ophir Optronics Solutions, Massachusetts, USA). The movement of the process beam relative to the sample surface was done by using a galvanometric scanner. Table 1 summarizes all related properties of the laser system used.

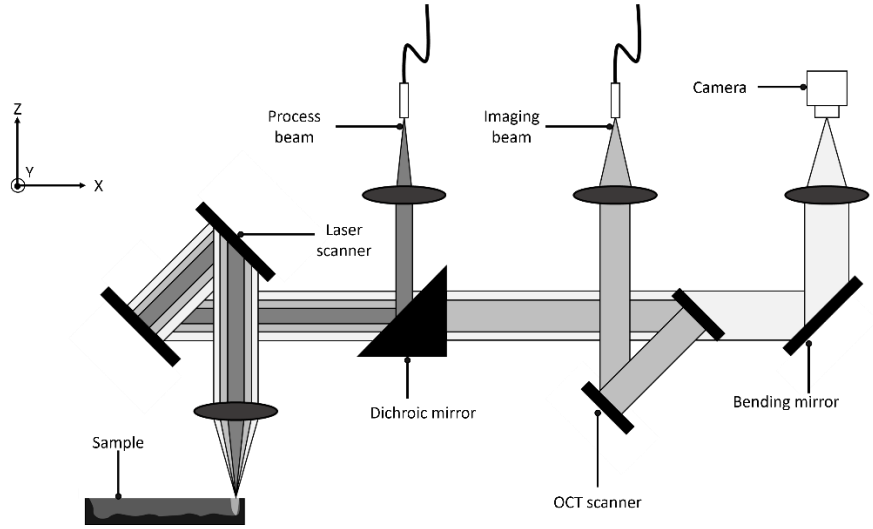

Figure 1 Schematic of the experimental setup used for this study

Table 1 Properties of the laser system

Property	Value
Laser brand and model	IPG YLS-2000/4000-SM-AMB
Maximum core power	2 kW
Maximum ring power	4 kW
Process beam wavelength	1070 nm
Central fiber core diameter	14 µm
Ring fiber diameter	$ø_{in}$=40 µm $ø_{out}$=100 µm
OCT brand and model	IPG LDD-700
Imaging beam wavelength	800—900 nm
Imaging beam power	<20 mW
Measurement frequency	Up to 250 kHz
Imaging beam diameter	34 µm

The keyhole depth was measured using an optical coherence tomography system (LDD-700, IPG Photonics, Cambridge, CA, USA), providing absolute distances as described in Webster et al., 2010. The OCT beam is directed coaxially through the same lens optics as the process beam, and onto the top surface of the material (see Figure 1), where it gets reflected and re-enters the system, and into the OCT detector. The OCT beam could be controlled separately with a dedicated scanner allowing to follow the process beam in complex trajectories as well as to apply beam alignment. The measurement is done at sampling rates of up to 250 kHz and with a measuring wavelength between 800 and 900 nm. The focal diameter of the OCT measuring beam is equal to ~34 µm, thus slightly smaller than the one of the single-mode beam. The main properties of the OCT system are summarized in Table 1. In order to compensate for the displacement of the deepest point in the keyhole opening due to the change in the process parameters, a calibration protocol was accomplished. The position of the OCT beam was offset with a certain lag distance with respect to the laser beam, following the reasoning and investigations as per Beck et al., 2021.

2.2. Material and characterization methods

EN AW-1050 aluminum alloy as a material generally used in electric mobility applications ranging from battery housings to electric drive parts was used throughout the study. Samples with a thickness of 5 mm were prepared. Following the laser welding of the samples and the in-situ OCT acquisitions of the keyhole depths, characterization via metallographic analysis was done. Weld seams were cut to produce cross-sectional samples, which were later grinded, polished, and chemically etched to reveal the melt track. Finally, the etched samples were examined using optical microscopy (Quick Vision Pro, Mitutoyo Corporation, Kawasaki, Japan).

Figure 2 (a) shows a schematic of a metallographic cross-section from which the cross-sectional weld depth h can be extracted. Three cut sections have been done at one quarter, two quarters, and three quarters of the weld bead length, as seen in Figure 2 (b). The average and the standard deviation of the measurements were calculated.

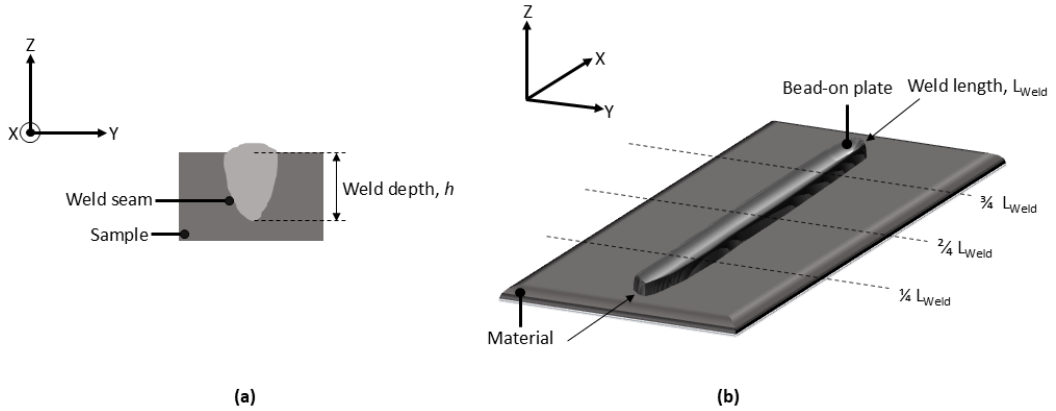

Figure 2 (a) Metallographic cross-section analysis; (b) Cut sections applied for each produced weld bead

2.3. Calibration protocol

During the welding process, the keyhole typically trails the laser beam. The exact location of the deepest point within the keyhole depends largely on the chosen process parameters, i.e. the laser core power, the laser ring power, and the welding speed. The spatial difference between the keyhole and the process beam necessitates an offset of the OCT beam with respect to the process beam. Accordingly, the lag distance in this study was defined as the distance between the leading process beam and the OCT beam, corresponding to the spatial offset of the OCT beam. For this, the calibration protocol was developed to accurately align the OCT beam spatially and temporally within the keyhole.

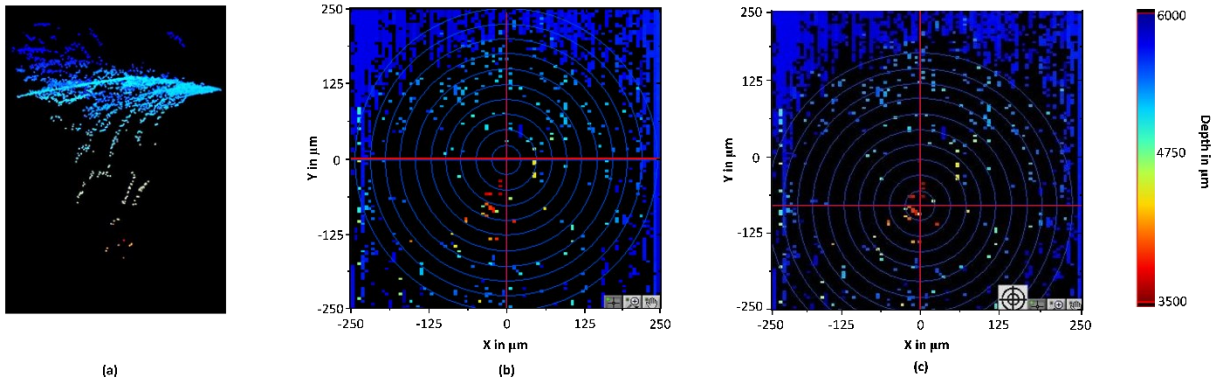

Figure 3 (a) An example of a 3D keyhole point cloud used in lag distance adjustment. (b) OCT beam position at the origin, and (c) OCT beam position towards the deepest points of the keyhole as depicted by the crosshair

The calibration protocol starts with a series of surface scanning of the morphology of the keyhole, in real-time during the weld process. The primary goal is to identify the lag distance and iteratively optimize it between one surface scan and the subsequent one. For each surface scan, a 3D depth map of the approximate keyhole shape is generated, in the form of a point cloud. The depth map is crucial in locating the deepest point of the resulting keyhole. At the beginning of the calibration, and prior to the first surface scan, the OCT beam is typically positioned in the origin at the x–y, i.e. at the (0,0) position. Figure 3 (a) illustrates an example of a 3D keyhole point cloud acquired after the first surface scan. Figure 3 (b), instead, shows the x-y depth map of the acquired keyhole. The depth map includes a crosshair that intersects at the pre-chosen (0,0) position. The region corresponding to the deepest point of the keyhole can be identified by the presence of the red dots in the point cloud which represent the maximum depth according to the depth map color scale. The crosshair is then repositioned on this region and the coordinates in x,y directions are consequently extracted. This process is illustrated in Figure 3 (c). These coordinates constitute the lag distance of the OCT beam attributed to the subsequent surface scan.

The steps were executed to locate the deepest point of the keyhole and determine the coordinates of the OCT beam. They were repeated in the succeeding surface scans to progressively refine OCT beam spatial alignment. This defines the iterative approach of the calibration protocol. The keyhole was first scanned using a wide field of view (FOV) with a fixed temporal resolution. At the beginning, and for the first surface scan, FOV was kept large to assess the correct position of the keyhole. As the FOV was reduced, more data points from the keyhole profile were registered. Hence, the FOV was progressively reduced through successive iterations, focusing more precisely on the internal section of the keyhole. The effect of the FOV reduction is illustrated in Figure 4. The 3D point cloud in Figure 4 (a) exemplifies a result of a surface scan for a 2000 x 2000 µm FOV configuration. Figure 4 (b) and (c), instead, display the same result of the previous scan surface, with narrower FOVs of 500 x 500 µm and 100 x 100 µm, respectively. As the FOV was restricted, the morphological details towards the keyhole's deepest point were enhanced, depicting with greater precision its inner part, thus leading to an optimized lag distance extraction from one scan to the subsequent one. Several iterations were required to achieve a fine calibration quality, during which the lag distance between the OCT and laser beams was continuously adjusted. The more iterations were executed, the minimum the effective distance between the deepest point of the keyhole and the OCT probe beam got. The lag distance extracted in the final surface scan of the keyhole was considered the effective lag distance and is subsequently used for the OCT-based keyhole depth measurement.

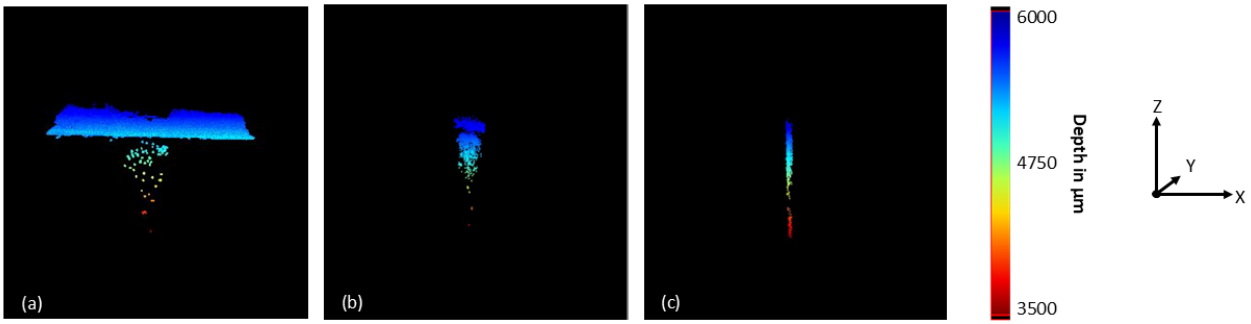

Figure 4 3D keyhole point cloud for different field of view configurations: (a) 2000 x 2000 µm, (b) 500 x 500 µm, and (c) 100 x 100 µm

In order to assess the impact of the calibration stage, the "rough alignment" and the "fine alignment" types were defined in this study. In the "rough alignment" protocol, the lag distance was adjusted over a total number of scans of up to three to quickly position the OCT beam within the deepest point of the keyhole. This approach makes the process more time-efficient and is relevant for industrial applications where rapid setup is prioritized. Nevertheless, it might lack positioning precision, as the OCT beam might scan regions within the keyhole slightly shifted from the deepest point, see Figure 5 (a). The "fine alignment" protocol involved up to twenty scans, with a lag distance optimized and adjusted for each step. The longer process ensured a much finer alignment of the OCT beam towards the deepest point in the keyhole, see Figure 5 (b). In such case, the outcome of the acquisition is expected to be more reliable and accurate, with a possible reduction of measurement error due to OCT beam misalignment. It can be noticed, for a rough alignment in Figure 5 (a), the measured depth is less than the one for a fine alignment in Figure 5 (b), as the OCT beam might have been positioned not in the proximity of the keyhole's deepest point.

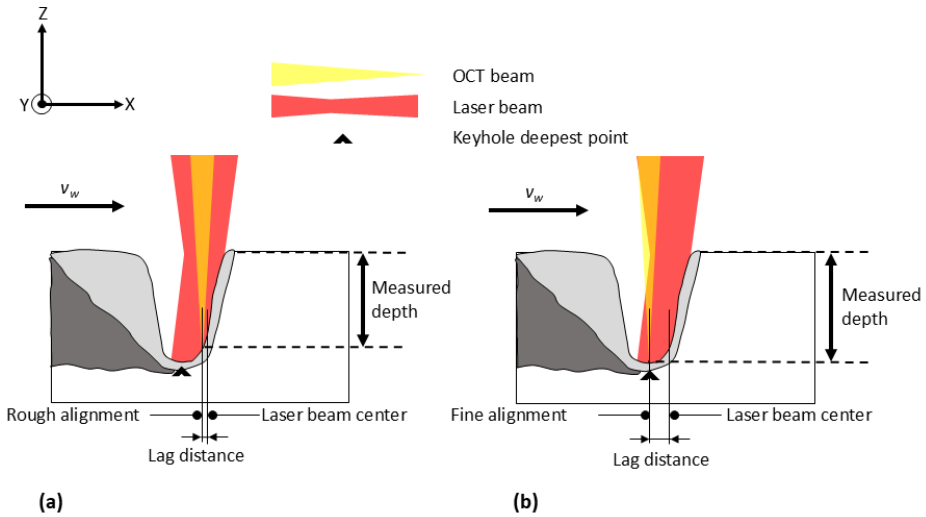

Figure 5 Schematic representations of (a) a rough alignment and (b) a fine alignment

2.4. Experimental design

In order to systematically investigate the effect of the different laser process parameters on the resulting keyhole and the relative in-situ OCT acquisition, a design of experiments with a 2^3 factorial approach was conducted. The design considers a low and a high weld speed v_w, being 100 and 800 mm/s, respectively. A high weld speed renders the keyhole very thin, thus, possibly leading to an unstable OCT acquisition and a difficulty in positioning the OCT beam itself within the resulting keyhole. Instead, the lower weld speed might help in enlarging the capillary aperture. The single-mode core power P_{Core} was kept unchanged during the experimental series, with a value of 1 kW. The ring power P_{Ring}, instead, varied between 0 and 2 kW. When P_{Ring} is absent, a very delicate process might be required to position efficiently the OCT beam of 34 µm in the keyhole that results from the single-mode core beam of 40 µm. The integration of a ring power, instead, leads to a widening of the keyhole and the melt pool (Galbusera et al., 2024). The chosen combinations of the process parameters would achieve different keyhole shapes, volumes, positions, and tilts, eventually leading to an understanding of OCT applicability and sensitivity for welding processes. Through the experiments, relative lag distances for both alignments were obtained, that vary for all the different combinations of process parameters. Once lag distances are identified, and for each laser set of parameters, two in-situ OCT weld depth acquisitions were performed, one with the 'fine alignment' lag distance, and another with the 'rough alignment' lag distance. The cross-sectional weld depth (h) was measured through cross-sections. The average of the keyhole depth measured by the OCT system (KHD) was registered for each experimental run. Bead-on plate tracks with 20 mm were produced in ambient atmosphere without a shielding gas. All experiments were done in the respective focal plane of the laser beam, pre-positioned on the top surface of the material. Table 2 summarizes fixed and variable parameters in this design of experiments.

Table 2 Variable and fixed factors of the experimental campaign

Fixed parameters	
Process gas	None
Focal position Δz	0 mm
Core power P_{Core}	1 kW
Weld length L_{weld}	20 mm
Variable parameters	
Ring power P_{Ring}	0; 2 kW
Weld speed v_w	100; 800 mm/s
OCT alignment	Rough; fine

3. Results and discussion

3.1. Weld cross-sections

Figure 6 (a) illustrates the metallographic cross-sections with respect to the process parameters. Figure 6 (b) shows the variations of cross-sectional weld depths. It can be seen that a lower weld speed v_w of 100 mm/s yields in a deeper weld seam profile directly related to a deeper keyhole. For example, for P_{Ring} = 0 kW, increasing the weld speed from 100 mm/s to 800 mm/s led to a decrease in h from around 1.59 mm to around 0.75 mm. Concerning the ring beam, when the ring power was adopted, a considerable enlargement was seen not only from the top of but all over the weld section. In addition, the ring power contributed to the depth of the weld. For example, at a fixed v_w = 100 mm/s, h was measured to be approximately 3.33 mm and 1.59 mm for a P_{Ring} at 2 kW and 0 kW, respectively.

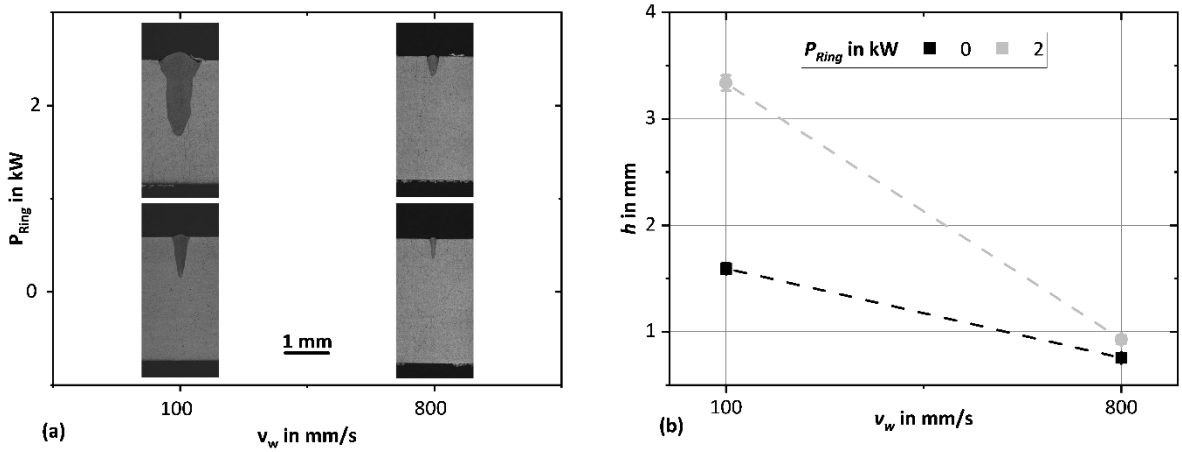

Figure 6 Influence of the process parameters on (a) the weld seam from one of the metallographic cross-sections and (b) the experimental weld depth h; the size of the standard deviation bars is comparable to the measurement icons

The lowest cross-sectional weld depth h value was obtained when using the single-mode core only (i.e. P_{Ring} = 0 kW) at the highest weld speed v_w = 800 mm/s. This combination of process parameters is related to the low laser energy provided by the laser beam to the metal. The total laser energy absorbed by the material is inversely proportional to weld speed and proportional to laser power (Banat et al., 2020), which proves the enlarged and deeper keyhole. Overall, the metallographic cross-sections revealed that a high weld speed combined with no ring power led not only to a shallower but also a narrower keyhole.

3.2. OCT signal behaviour

Figure 7 (a) and (b) illustrate OCT acquisitions for welds performed with only the single-mode core power of 1 kW, at a weld speed of 800 mm/s, for rough and fine alignments, respectively. This combination of process parameters led to the shallowest and narrowest keyhole observed. The green line represents the tracking algorithm that identifies the maximum depth positions used to monitor the keyhole depth along the weld line, while the white dots represent the returned signals within the OCT detector. Each alignment process was associated with a lag distance, varying with the different set of parameters. For this case, the fine alignment resulted in a lag distance of approximately 15 µm after seventeen iterations, whereas the rough alignment used a lag distance of approximately 100 µm after three iterations. The OCT-based keyhole depth measured at 0.44 mm for rough alignment and 0.86 mm for fine alignment. The standard deviations associated with the measured keyhole depth were 0.36 mm and 0.17 mm, respectively

In order to investigate the effect of the ring beam profile, Figure 7 (c) and (d) provide OCT acquisitions for welds with P_{Ring} = 2 kW at a weld speed v_w = 800 mm/s, again for rough and fine alignments, respectively. In this case, the lag distance that after a fine alignment was 67 µm with seven iterations. Instead, for the rough alignment, the lag distance was determined to be approximately 170 µm, after two iterations. The OCT-based keyhole depths from the OCT acquisitions were 0.8 mm (rough) and 0.96 mm (fine), with standard deviations of 0.07 mm and 0.03 mm, respectively.

In all cases, the OCT keyhole depth was higher whenever a fine alignment process was performed, confirming the accuracy of the OCT beam alignment towards the deepest point of the keyhole. Moreover, fine alignment required fewer iterations when the ring beam was added—seventeen iterations using the single-mode beam versus seven—indicating an easing of

the process with the ring beam. In contrast, the rough alignment of the OCT beam led to a considerable underestimation of the keyhole depth. The difference in the measurements obtained highlights the sensitivity of the OCT and emphasizes the importance of precise alignment. Additionally, the difference in the measured keyhole depth between a rough alignment and a fine alignment was decreased whenever the ring power was adopted due to further accessibility of the OCT beam in the deepest region. The additional ring profile led to a wider keyhole. The enlargement within the keyhole eased the alignment process due to the flattening of the keyhole's bottom. This observation is consistent with the decrease in the number of iterations in both rough and fine alignments, whenever a ring power was adopted.

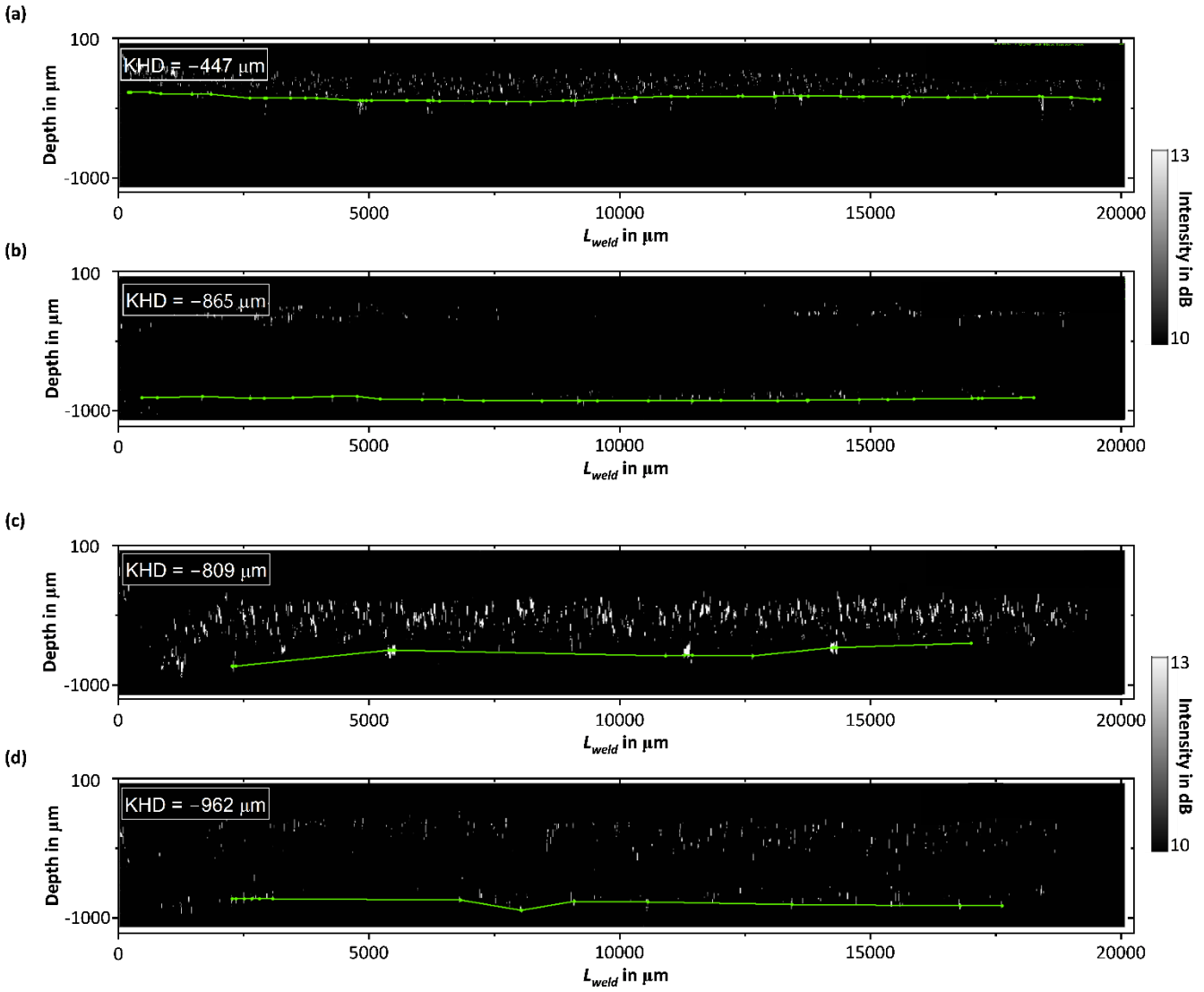

Figure 7 Resulting OCT depth measurements for: a single-mode core power of 1 kW with no ring power at 800 mm/s after (a) a rough calibration and (b) a fine calibration; a single-mode core power of 1 kW, a ring power of 2 kW, at 800 mm/s after (c) a rough calibration and (d) a fine calibration; the green line represents the identified maximum depth profile

3.3. Comparative analysis between cross-section depths and OCT depth measurements

Figure 8 shows the comparative analysis of the cross-sectional weld depth to both the fine alignment and the rough alignment KHDs. For the sake of simplicity and comparison, they have been denoted as KHD_F and KHD_R, respective of the fine and rough alignments. Considering welding with only the single-mode core beam, i.e. P_{Ring} = 0 kW, with a weld velocity of 100 mm/s, the cross-sectional weld depth was 1.59 mm. KHD_F was 1.63 mm, while KHD_R was 1.28 mm. For the same laser

core and ring power, with a weld velocity of 800 mm/s instead, h was equal to 0.75 mm, while KHD_F and KHD_R were 0.78 mm and 0.44 mm, respectively.

For a rough alignment, a significant error is present between the depths measured from cross-sections and from the OCT acquisitions. Also, the standard deviations increased in value and were comparatively higher than the ones obtained with fine alignment. This owes to the fact that the laser beam and the OCT beam lay in the same order of magnitude, being 40 µm and 34 µm respectively. Thus, the probability of positioning the OCT beam far from the deepest point of the keyhole is significantly higher, if the lag distance was not finely tuned, which in turn renders the measurements unreliable and flawed. Furthermore, in some cases, KHD_F was found to be slightly higher value than to h. This may be due to multiple reflection phenomenon, which may play a significant role in the case of small-measured depths (Boley et al, 2014).

With a fine alignment, the weld depth was measured accurately, even for the narrowest and shallowest keyholes, i.e. keyholes resulting from welds with only the single-mode beam, at high weld speeds. The difference between the measured keyhole depth from the cross-sections and from the OCT acquisition was negligible, and thus reliable for industrial standards.

It can be seen from Figure 8 that a lower difference in value between KHD_R and h was present whenever a ring power was adopted in the weld process. The role of the ring profile in flattening the keyhole's overall section eased the placement of the OCT beam towards the keyhole's deepest point. Although limited iterations were accomplished, following a rough alignment process when a ring power is adopted led to a better OCT beam positioning towards the keyhole's deepest point, resulting in a smaller error margin, thus validating the contribution of the ring profile.

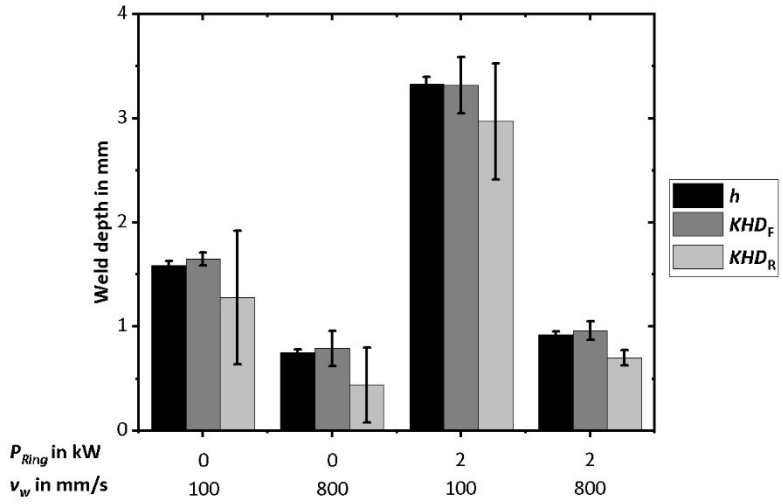

Figure 8 Comparison of OCT depth measurements resulting from both a rough (KHD_R) and a fine calibration (KHD_F) and depths from metallographic cross sections (h). Error bars represent standard deviations of depths measured by each technique.

4. Conclusion

This paper presented the use of OCT in-situ keyhole depth measurements with a novel laser beam source incorporating a single-mode core with a ring beam. The work showed that through a lengthy and detailed fine calibration stage, the OCT system can measure keyhole depths produced by a single-mode laser beam at welding speeds up to 800 mm/s. The use of ring beam profiles makes the calibration stage shorter by providing a wider keyhole opening. In all cases, the use of the fine calibration stage was found to decrease the variability of the measurements as well as the error with respect to the melt track depth measured on the metallographic cross sections. Future investigations will focus on the automatization of the process in a way to mitigate the calibration process which can be considered as time and cost consuming for industrial applications.

References

Demir, A.G., Kriegler, J., Fortunato, A., Caprio, L., Geiger, C., Hille, L., Kick, M.K., Ascari, A., Liverani, E. and Zaeh, M.F., 2023. Challenges and opportunities for laser applications in electric vehicle manufacturing. *Selected Topics in Manufacturing: Emerging Trends from the Perspective of AITeM's Young Researchers*, pp.219—253.

Xie, G., Wang, S., Zhang, Y., Hu, B., Fu, Y., Yu, Q. and Li, Y., 2023. An efficient method for laser welding depth determination using optical coherence tomography. *Sensors*, *23*(11), p.5223.

Webster, P.J., Leung, B.Y., Joe, X.Z., Anderson, M.D., Hoult, T.P. and Fraser, J.M., 2010, February. Coaxial real-time metrology and gas assisted laser micromachining: process development, stochastic behavior, and feedback control. In *Micromachining and microfabrication process technology XV* (Vol. 7590, pp. 15—24). SPIE.

Mittelstaedt, C., Mattulat, T., Seefeld, T. and Kogel-Hollacher, M., 2019. Novel approach for weld depth determination using optical coherence tomography measurement in laser deep penetration welding of aluminum and steel. *Journal of Laser Applications*, *31*(2).

Blug, A., Carl, D., Hoefler, H., Abt, F., Heider, A., Weber, R., Nicolosi, L. and Tetzlaff, R., 2011. Closed-loop control of laser power using the full penetration hole image feature in aluminum welding processes. *physics procedia*, *12*, pp.720—729.

Miyagi, M., Kawahito, Y., Kawakami, H. and Shoubu, T., 2017. Dynamics of solid-liquid interface and porosity formation determined through x-ray phase-contrast in laser welding of pure Al. *Journal of Materials Processing Technology*, *250*, pp.9—15.

Boley, M., Berger, P., Webster, P.J., Weber, R., Van Vlack, C., Fraser, J. and Graf, T., 2013, October. Ivestigating the weld depth behaviour using different observation techniques: X-ray, inline coherent imageing and highspeed observation during welding ice. In *International Congress on Applications of Lasers & Electro-Optics* (Vol. 2013, No. 1, pp. 22—27). Laser Institute of America.

Dorsch, F., Harrer, T., Haug, P. and Plasswich, S., 2016, October. Process control using capillary depth measurement. In *International Congress on Applications of Lasers & Electro-Optics*. AIP Publishing.

Schmoeller, M., Stadter, C., Liebl, S. and Zaeh, M.F., 2019. Inline weld depth measurement for high brilliance laser beam sources using optical coherence tomography. *Journal of Laser Applications*, *31*(2).

He, G., Gao, X., Li, L. and Gao, P., 2024. OCT monitoring data processing method of laser deep penetration welding based on HDBSCAN. *Optics & Laser Technology*, *179*, p.111303.

Sokolov, M., Franciosa, P., Sun, T., Ceglarek, D., Dimatteo, V., Ascari, A., Fortunato, A. and Nagel, F., 2021. Applying optical coherence tomography for weld depth monitoring in remote laser welding of automotive battery tab connectors. *Journal of Laser Applications*, *33*(1).

Hollatz, S., Hummel, M., Jaklen, L., Lipnicki, W., Olowinsky, A. and Gillner, A., 2020. Processing of keyhole depth measurement data during laser beam micro welding. *Proceedings of the Institution of Mechanical Engineers, Part L: Journal of Materials: Design and Applications*, *234*(5), pp.722—731.

Beck, T., Bantel, C., Boley, M. and Bergmann, J.P., 2021. Oct capillary depth measurement in copper micro welding using green lasers. *Applied Sciences*, *11*(6), p.2655.

Galbusera, F., Borzoni, G., D'Arcangelo, S., Caprio, L., Previtali, B. and Demir, A.G., 2024. The effect of in-source spatial beam shaping on the laser welding of e-mobility metals and alloys. Procedia CIRP, 124, pp.20—23.

Banat, D., Ganguly, S., Meco, S. and Harrison, P., 2020. Application of high power pulsed nanosecond fibre lasers in processing ultra-thin aluminium foils. *Optics and Lasers in Engineering*, *129*, p.106075.

Boley, M., Webster, P., Heider, A., Weber, R. and Graf, T., 2014, October. Investigating the keyhole behavior by using x-ray and optical depth measurement techniques. In *ICALEO 2014: 33nd International Congress on Laser Materials Processing, Laser Microprocessing and Nanomanufacturing* (pp. 426-430). AIP Publishing.